

Supporting information: Influence of Disorder and Anharmonic Fluctuations on the Dynamical Rashba Effect in Purely Inorganic Lead-Halide Perovskites

Arthur Marronnier,^{*,†} Guido Roma,[‡] Marcelo Carignano,[¶] Yvan Bonnassieux,[†]
Claudine Katan,[§] Jacky Even,^{||} Edoardo Mosconi,[⊥] and Filippo De Angelis^{⊥,#}

[†]*LPICM, CNRS, Ecole Polytechnique, Université Paris-Saclay, 91128 Palaiseau, France*

[‡]*DEN - Service de Recherches de Métallurgie Physique, CEA, Université Paris-Saclay,
91191 Gif sur Yvette, France*

[¶]*Qatar Environment and Energy Research Institute, Hamad Bin Khalifa University, P.O.
Box 5825, Doha, Qatar*

[§]*Univ Rennes, ENSCR, INSA Rennes, CNRS, ISCR (Institut des Sciences Chimiques de
Rennes) – UMR 6226, F-35000 Rennes, France*

^{||}*Univ Rennes, INSA Rennes, CNRS, Institut FOTON — UMR 6082, F-35000 Rennes,
France*

[⊥]*Computational Laboratory for Hybrid/Organic Photovoltaics (CLHYO), CNR-ISTM, Via
Elce di Sotto 8, I-06123 Perugia, Italy*

[#]*D3-CompuNet, Istituto Italiano di Tecnologia, Via Morego 30, 16163 Genova, Italy*

E-mail: arthur.marronnier@polytechnique.edu

Introduction

We provide, in this Supporting Information file, further data on the band structure of the snapshots extracted from the MD simulation and some further analysis of the Rashba parameter α_R and other relevant quantities related to the spin texture throughout the 5 ps of the simulation on which we focused our study.

Band structure

In the main manuscript we showed the band gap around the Γ point of the BZ along the MD simulation. The corresponding highest occupied valence band and lowest unoccupied conduction band are shown in the six panels (a-f) of figureS1. As for figure 5 of the main manuscript, showing the band gap, the bands are referred to the value at Γ for the same snapshot, i.e., we show : $\epsilon_i(\mathbf{k}, t) - \epsilon_i(\Gamma, t)$, where i labels the valence band top (VBT) or the conduction band minimum (CBM).

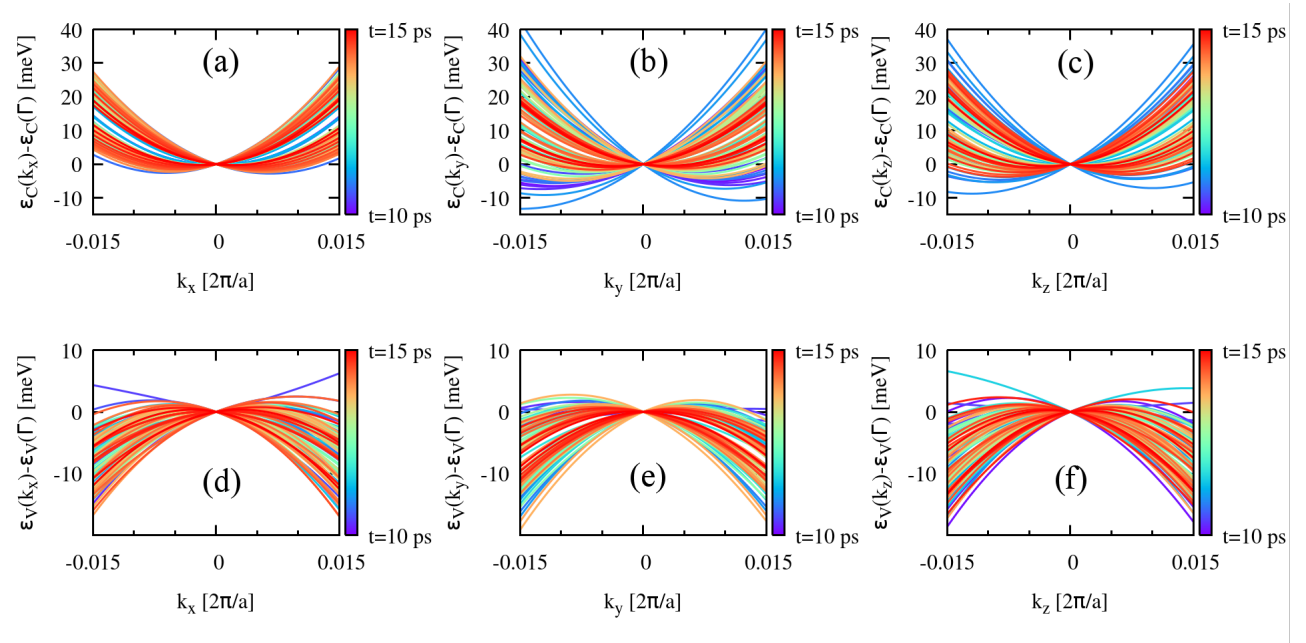


Figure S1: Band structure along the three reciprocal space direction, \mathbf{k}_x , \mathbf{k}_y , \mathbf{k}_z , for the first unoccupied conduction band (panels a-c) and the last occupied valence one (panels d-e).

These bands were obtained by assuming a parabolic shape passing through the three calculated \mathbf{k} points for each cartesian direction. The 7 \mathbf{k} -points (Γ belongs to the three directions) are shown in Table 1

Table 1: The \mathbf{k} points of the Brillouin zone used in the 50 band structure calculations in units of $\frac{2\pi}{a_{x,y,z}^i}$ where $a_{x,y,z}^i$ are the lattice parameters for snapshot i in one of the three cartesian direction, x , y or z .

Point number	x	y	z
1	0.1	0	0
2	0.05	0	0
3 (Γ)	0	0	0
4	0	0.05	0
5	0	0.1	0
6	0	0	0.05
7	0	0	0.1

It is the assumption of a parabolic shape that induces a slight time reversal symmetry breaking ($\epsilon_{\mathbf{k}} \neq \epsilon_{-\mathbf{k}}$). It allows to appreciate the small error associated with the calculation of the Rashba parameter α_R .

The bands are always referred to the value at Γ , because the time fluctuations of the bands themselves, and of the bandgap itself, are much larger than the energy splitting ΔE entering the definition of the Rashba parameter α_R . We show, as an indication of this, the evolution of the band gap throughout the 5 ps interval on which we have focused (figure S2). As can be seen, there is no sign of gap closure during the simulation.

Time correlation functions

We further investigated time correlation functions of the Rashba parameter and of spin related functions. Correlation functions between two functions of time $A(t)$ and $B(t)$ were calculated, along our 5 ps MD trajectory, as discrete sums:

$$C_{AB}(j) = \frac{1}{(M+1)} \sum_{i=0}^M A(i)B(i+j)$$

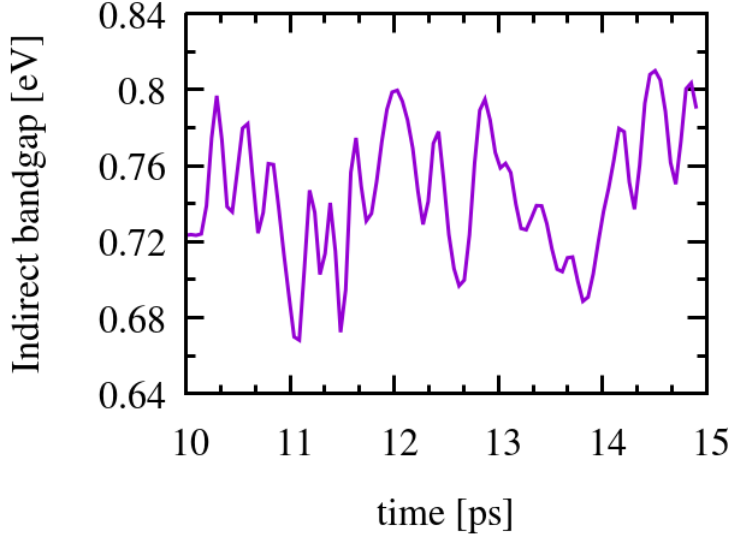


Figure S2: Evolution of the band gap in the time interval of 5 ps which was analyzed.

where i and j label the discrete snapshots of the simulation. We have checked the convergence with the number of points M used for averaging and found that for $M=11$ time correlation functions are sufficiently well converged; nevertheless we are aware that our 50 simulation snapshots represent a very small statistical sample and allow only qualitative considerations. First we show in figure S3 the autocorrelation function of the α_R parameter for the three cartesian directions for valence and conduction bands.

The fact that the correlation functions show a coherent monotonously decreasing behavior over a few picoseconds means that the α_R parameter is still correlated on this time scale. As expected the conduction band shows stronger Rashba splitting, in particular along \mathbf{k}_y and \mathbf{k}_z directions. The largest effect is expected when α_R is large for both valence and conduction bands. For this reason we calculated the cross correlation function between the α_R parameters of valence and conduction bands, $C_{\alpha_R^V \alpha_R^C}(t)$, which is shown in figure S4.

Here, again, we find a clear decreasing trend, sign of a correlation between valence and conduction Rashba parameters over a time scale of the same order as for the autocorrelation functions.

Let us now switch to correlation functions related to the spin texture. We consider the

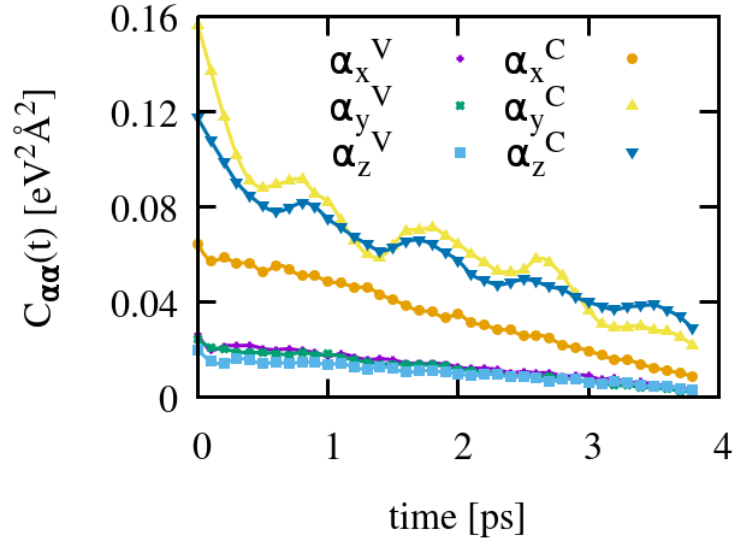


Figure S3: Time autocorrelation function of the Rashba α_R parameter for the three cartesian directions for valence and conduction bands.

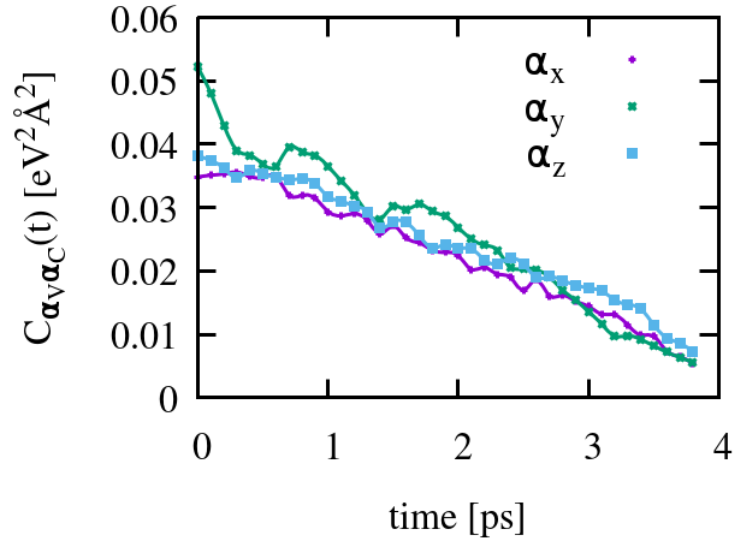


Figure S4: Time cross-correlation function for the valence/conduction Rashba α_R parameters for the three cartesian directions.

function shown on figure 2c of the main manuscript; we could call it the spin-matching-function:

$$S_{match}(t, \mathbf{k}) = \sum_{i=1,3} \langle \sigma_i \rangle_V^{\mathbf{k}} \cdot \langle \sigma_i \rangle_C^{\mathbf{k}}$$

where the expectation values of the Pauli spin matrices $\langle \sigma_i \rangle_{V/C}^{\mathbf{k}}$ are taken over the spinor valence/conduction wave function $\psi_{\mathbf{k}}^{V/C}(\mathbf{r}, t)$, at point \mathbf{k} of the BZ and at time t . We have not interpolated the spin texture along the \mathbf{k}_{xyz} directions, so we consider only the calculated \mathbf{k} points.

We have checked the autocorrelation functions for $S_{match}(t, \mathbf{k})$ at the Γ point and at one \mathbf{k} point in each of the cartesian directions, as well as the average of S_{match} over the 7 calculated \mathbf{k} -points: in all cases a similar decreasing trend is observed. The same holds for the cross correlation functions between α_R and S_{match} . Examples are shown in figure S5.

However, we are interested in knowing if the spin matching function, and thus presumably the recombination rate, is reduced at a finite \mathbf{k} point with respect to the zone center. For this we consider $S_{match}(t, \mathbf{k}) - S_{match}(t, \Gamma)$; the corresponding time autocorrelation function is shown in figure S6, which clearly shows that this difference gets uncorrelated in a much shorter time than the α_R parameter. This suggests that either this reduction is too small to be appreciated, and/or it is indeed completely uncorrelated with the Rashba effect.

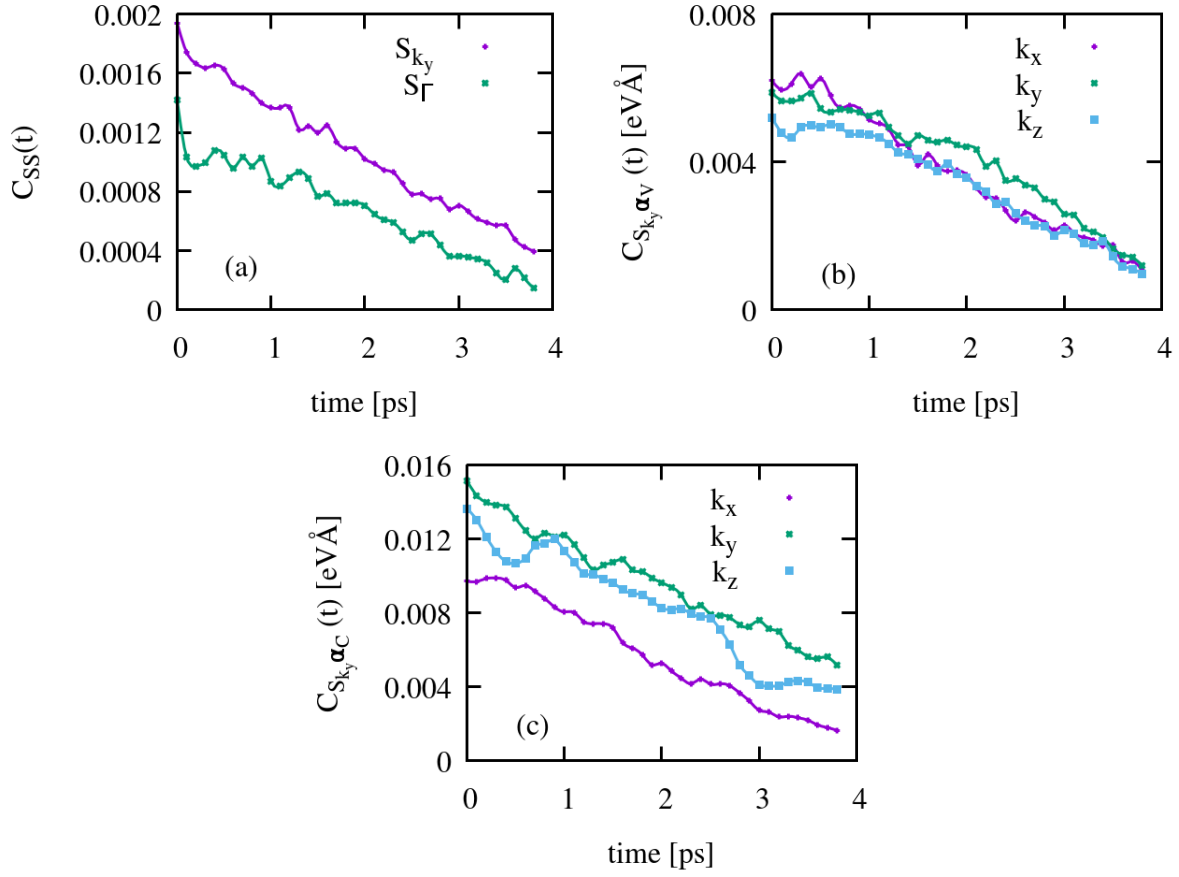


Figure S5: Panel (a): time autocorrelation function of the spin matching function (see text) S_{match} at Γ and a point along k_y . Panels (b,c) : cross correlation functions between the spin-matching-function and the Rashba α_R parameter of the valence (b) and conduction (c) bands.

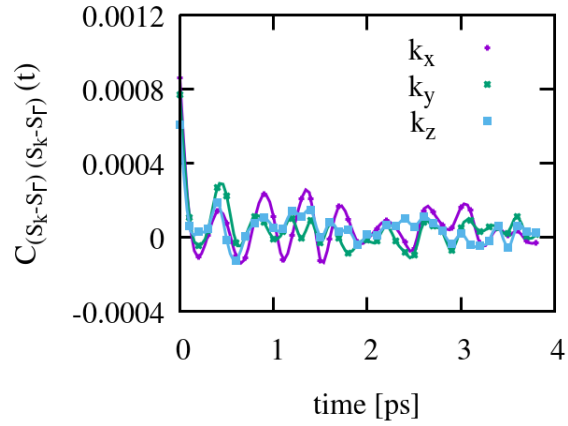


Figure S6: Time autocorrelation function of the difference between spin-matching-functions at Γ and at a finite \mathbf{k} point along the three cartesian directions in the BZ.

Influence of Disorder and Anharmonic Fluctuations on the Dynamical Rashba Effect in Purely Inorganic Lead-Halide Perovskites

Arthur Marronnier,^{*,†} Guido Roma,[‡] Marcelo Carignano,[¶] Yvan Bonnassieux,[†]
Claudine Katan,[§] Jacky Even,^{||} Edoardo Mosconi,[⊥] and Filippo De Angelis^{⊥, #}

[†]*LPICM, CNRS, Ecole Polytechnique, Université Paris-Saclay, 91128 Palaiseau, France*

[‡]*DEN - Service de Recherches de Métallurgie Physique, CEA, Université Paris-Saclay,
91191 Gif sur Yvette, France*

[¶]*Qatar Environment and Energy Research Institute, Hamad Bin Khalifa University, P.O.
Box 5825, Doha, Qatar*

[§]*Univ Rennes, ENSCR, INSA Rennes, CNRS, ISCR (Institut des Sciences Chimiques de
Rennes) – UMR 6226, F-35000 Rennes, France*

^{||}*Univ Rennes, INSA Rennes, CNRS, Institut FOTON — UMR 6082, F-35000 Rennes,
France*

[⊥]*Computational Laboratory for Hybrid/Organic Photovoltaics (CLHYO), CNR-ISTM, Via
Elce di Sotto 8, I-06123 Perugia, Italy*

[#]*D3-CompuNet, Istituto Italiano di Tecnologia, Via Morego 30, 16163 Genova, Italy*

E-mail: arthur.marronnier@polytechnique.edu

Abstract

Doping organic metal-halide perovskites with cesium could be the best solution to stabilize highly-efficient perovskite solar cells. The understanding of the respective roles of the organic molecule, on one hand, and the inorganic lattice, on the other, is thus crucial in order to be able to optimize the physical properties of the mixed-cation structures. In particular, the study of the recombination mechanisms is thought to be one of the key challenges towards full comprehension of their working principles. Using molecular dynamics and frozen phonons, we evidence sub-picosecond anharmonic fluctuations in the fully inorganic CsPbI₃ perovskite. We reveal the effect of these fluctuations, combined with spin-orbit coupling, on the electronic band structure, evidencing a dynamical Rashba effect. Our study shows that under certain conditions space disorder can quench the Rashba effect. As for time disorder, we evidence a dynamical Rashba effect which is similar to what was found for MAPbI₃ and which is still sizable despite temperature disorder, the large investigated supercell, and the absence of the organic cations' motion. We show that the spin texture associated to the Rashba splitting cannot be deemed responsible for a consistent reduction of recombination rates, although the spin mismatch between valence and conduction band increases with the ferroelectric distortion causing the Rashba splitting.

Keywords

inorganic perovskite solar cells, anharmonicity, cesium, phonons, DFT, molecular dynamics, Rashba

Introduction

Fully inorganic metal-halide perovskites have attracted more and more attention in the past two years as they have showed promising efficiencies (record efficiency of 13.4% for quantum dot devices¹ and of 15.07% recently reported for a thin film²) and as cesium doping has proven to be a good way to improve the environmental stability of hybrid metal-halide perovskites.³ Moreover, a better understanding of the physical properties of fully inorganic halide perovskites is needed in order to further understand, by contrast, the role of the organic cation in their hybrid cousins.

In general, the enthusiasm for metal-halide perovskites can be explained by their exceptional optoelectronic properties, whether it be their optical properties,⁴⁻⁷ the long lifetimes of both electrons and holes⁸⁻¹⁰ and the high mobility in these materials.^{10,11} Another remarkable feature of these materials is the fact that they present good absorption and charge generation properties,^{12,13} but to fully exploit this for solar cells one should be able to control all the factors that limit overall recombination rates. If the former —absorption— could be explained in particular by the materials' direct band gap, for the latter —recombination— one expects high values for both the radiative (direct band gap) and non-radiative recombination (high density of defects). As for defects, one should note that charge separation could be actually eased in these materials through halide ionic migration^{14,15} which could either favour exciton screening¹⁶ or give birth to local screening domains.^{17,18}

Concerning radiative recombination, which has been indeed shown to be relatively high,¹⁹ one should take into account the interplay of spin and orbital degrees of freedom, which are of important magnitude in these materials because of the presence of the heavy lead atoms. In particular, the giant spin-orbit coupling (SOC) that was reported in these materials²⁰ is expected to be at the origin of Rashba-like splittings.²¹⁻²⁴ Such splittings correspond to the lift of the electronic bands' spin degeneracy in the presence of SOC and time reversal symmetry when the inversion symmetry is broken in the crystal.^{25,26} Assuming long-range polar distortions of the perovskite lattice, it has been speculated that these band splittings

can drastically impact the recombination rates by limiting direct transitions between the valence and conduction bands. This impact was theoretically estimated by Zheng *et al.* to contribute to a reduction of the recombination rates reaching up to two orders of magnitude.⁹ However, the existence of long-range polar distortions of iodide-based perovskite lattices is still debated, the influence of Rashba-like spinor band splittings could be more subtle and rather related to local lattice distortions. Moreover, very recent works^{27,28} question the role of Rashba splitting in MAPbI₃ (MA=methylammonium), where the inversion symmetry breaking is associated to the orientation of methylammonium ions. The Rashba effect can influence carrier transport in halide perovskite also by modifying the carrier mobility, due to modified electron-phonon scattering.^{29,30}

Etienne *et al.*³¹ investigated by DFT-based molecular dynamics the interplay of electronic and nuclear degrees of freedom in the prototype MAPbI₃ perovskite and revealed a dynamical Rashba effect. They reported the influence of temperature and found a spatially local Rashba effect with fluctuations at the subpicosecond time scale, that is to say on the scale of the MA cation motion. Although this time scale is much smaller than the carrier lifetimes, apart from directly affecting radiative recombination probabilities, it could influence the kinetic path for electron-hole recombination.³² It is worth pointing out that this numerical demonstration by Etienne and coworkers was based on MAPbI₃ structures preserving centrosymmetry on the average. They noticed that the Rashba splitting can be quenched when reaching room temperature but also when using larger supercells (up to 32 MAPbI₃ units, i.e., 3 nanometers cells) representing a higher and more realistic spatial disorder. The effect is still debated,³³ but an experimental evidence of dynamical Rashba splitting in MAPbI₃ was recently reported.³⁴

The local and dynamical nature of polar distortions may weaken the influence of Rashba-like spinor splittings by comparison to long range and static polar distortions. However the lack of long range correlations between local polar distortions could be compensated by the unusually strong amplitudes of the atomic motions. The strong anharmonicity of the per-

ovskite lattice is a general feature of this new class of semiconductors,³⁵ that was pointed out experimentally very early by inelastic neutron scattering in the context of inorganic halide perovskites³⁶ and that shall give rise to at least two characteristic experimental signatures: large and anisotropic Debye-Waller factors in diffraction studies^{37,38} and a so-called quasielastic central peak observed either in inelastic neutron or Raman scattering studies simultaneously with highly damped phonons.^{39,40} However, the strong perovskite lattice anharmonicity is not expected to affect only zone center polar optical modes, but also acoustic modes or optical modes located at the edges or the Brillouin zone and related to non-polar antiferrodistortions.³⁵ The previously mentioned experimental signatures (Debye-waller factors, phonon damping and central peaks by inelastic neutron or Raman scattering studies) can hardly be considered as unambiguous experimental proofs of the existence of strongly anharmonic polar fluctuations. Nowadays direct experimental investigations of the dielectric response give useful indications about the influence of lattice polar distortions^{41,42} and the importance of the Fröhlich interaction⁴³ for electron-phonon coupling processes,⁴⁴ but do not directly probe the anaharmonicicity of polar distortions. Numerical simulations are therefore still useful tools that already allowed showing the presence of anharmonicity features in CsPbI₃,^{45,46} leading to symmetry breaking minimum structures in the high temperature phases both at the edges and at the center of the Brillouin zone. MD simulations for CsPbBr₃ also suggested that the fluctuations in this material are mostly due to head-to head Cs motion and Br face expansion happening on a few hundred femtosecond time scale.⁴⁰

In that sense, large polar fluctuations of the perovskite lattice at the local scale may lead to two main effects: Rashba-like spinor splittings and strongly anharmonic polarons related to the Fröhlich interaction. We focus in the present contribution on the former aspect.

Results and Discussion

In this article, we aim to analyze the Rashba effect induced by the anharmonic double well and the influence of symmetry breaking that has been evidenced in the cubic phase of CsPbI_3 .^{45,46} In fact it was shown, using the frozen phonon method, that the highly symmetric cubic phase can be distorted to form two lower-symmetry structures with a slightly lower total energy (by a few meV). These two distorted structures, that we will call in the rest of the article A^+ and A^- , have no inversion symmetry and correspond to the two minimum structures of the double well-instability discussed in Ref. 45. They correspond to opposite ferroelectric distortions ($\eta > 0$ and $\eta < 0$) along a soft polar eigenmode of the centrosymmetric $Pm\bar{3}m$ ("S") structure, represented in Figure 1a, along the x -direction. Note that with rotational symmetry similar studies could be done on the two other eigenmodes corresponding to distortions along the two remaining Cartesian axes (y and z given our labeling). The first aim of the study here is to look at the possible formation of " A^+ domains" and " A^- domains", both in space (supercells) and in time (Car-Parrinello molecular dynamics "CPMD").

Then, we analyze in detail the dynamical Rashba effect induced by the time dynamics of the oscillations between structure A^+ and structure A^- through the highly symmetric structure S ($\eta = 0$). This study is done on CPMD trajectories obtained from Ref. 47

Spatial disorder

First, the aim is to investigate the influence of spatial A^+/A^- domains in CsPbI_3 on its electronic band structure, in particular in terms of Rashba effect. Given that the eigenvector under study mostly corresponds to a distortion along one axis (here we considered the x-axis) we built supercells by doubling the unit cell either in the x direction or in the z direction. These $2 \times 1 \times 1$ and $1 \times 1 \times 2$ supercells are built putting together 2 unit cells: 1 unit cell in configuration A^+ (or x up), and another one in configuration A^- (or x down).

These supercells, representing modulated structures with the smallest possible period, are schematically shown in Figure 1a.

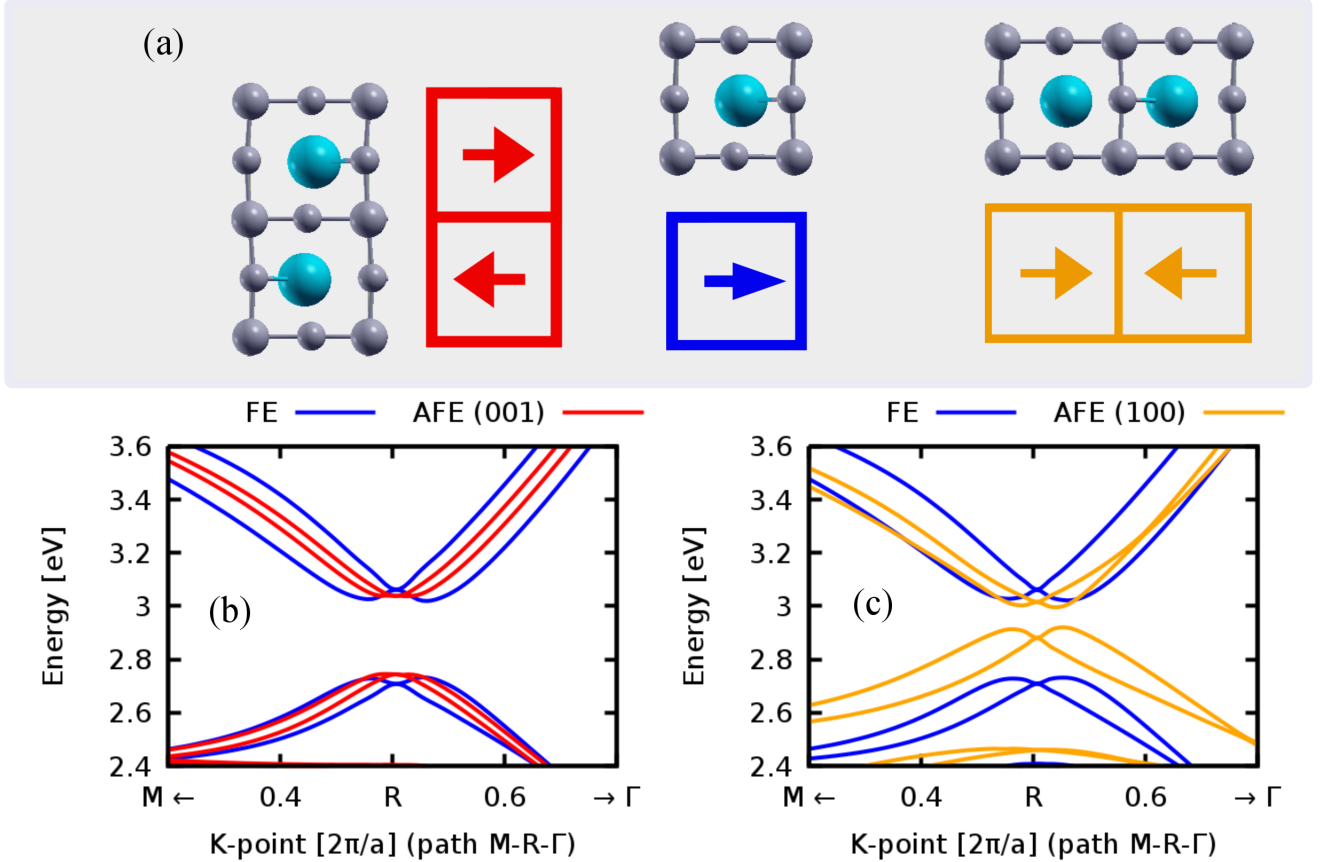


Figure 1: (a) Sketch of the atomic structure and schematic representations of the corresponding unit cells used to study the influence of spatial domains A^+/A^- or "x up"/"x down" on the electronic band structure (arrows represent displacement of Cs, the blue atom). (b,c) Electronic band structure (including SOC) of the $2 \times 1 \times 1$ (orange) and $1 \times 1 \times 2$ (red) anti-ferroelectric (AFE) configurations, both compared to the ferroelectric (FE) one (blue). The labelling of the k-points is referred to the BZ of the cubic unit cell.

The Rashba splitting obtained at the R point for a unit cell, in the minimum, symmetry-breaking structure is shown in Figure 1, the blue curve in panels a and b. When doubling the cell along z (resp. x), the R point folds onto the S point (resp. T point), using the orthorhombic convention (in the figure we kept the labels of the cubic unit cell). For this ordered, static reference structure we find energy splittings of 42 meV (57 meV with LDA) and 24 meV (40 meV with LDA) between the Γ point and, respectively, the conduction band

minimum and valence band maximum. In order to give an estimate of the Rashba splitting taking into account the effect both in energy and in the k-space, we calculated the commonly used α parameter as defined in Ref. 31:

$$\alpha_{C,V} = \frac{\Delta E_{C,V}}{2\Delta k_{C,V}} \quad (1)$$

where $\Delta E_{C,V}$ is the energy difference between the first (resp. last) two bands of the conduction (resp. valence) bands and $\Delta k_{C,V}$ the splitting of the minimum (resp. maximum) in the k-space. For the reference static, highly ordered structure we found α values of 3.04 (4.09 with LDA) eV.Å and 2.75 (2.01 with LDA) eV.Å for the conduction and the valence bands, respectively. These values are comparable to those reported in Ref. 31 in the case of polar MAPbI₃: 3.17 eV.Å and 1.17 eV.Å respectively. Note that so far the highest values found in ferroelectric materials for the Rashba parameter are 4.2-4.8 eV.Å for GeTe.^{48,49}

The results for the two modulated structures are shown in Figures 1b and 1c. Whereas no Rashba effect is found in the case of a modulation orthogonal to the direction of symmetry breaking, a band splitting around the valence band maximum and the conduction band minimum is found for a modulation parallel to the direction of symmetry breaking. We found α values of 1.98 (0.58 with LDA) eV.Å and 2.97 (2.18 with LDA) eV.Å for the conduction and valence bands, respectively.

In general, the Rashba splitting in the band structure of a two-dimensional system results from the combined effect of atomic spin-orbit coupling and asymmetry of the potential in the direction (here x) perpendicular to the two-dimensional plane, causing a loss of inversion symmetry. In the case of a modulation orthogonal to the direction of symmetry breaking ($1 \times 1 \times 2$ supercell), the symmetry along x is respected on average: the inversion symmetry is kept and the Rashba splitting vanishes. We expect then that the quenching of the Rashba effect results from a competition between parallel and orthogonal modulations: the former keeps the Rashba effect, while the latter tends to cancel it.

According to Rashba model hamiltonians the spin texture is such that the top of the

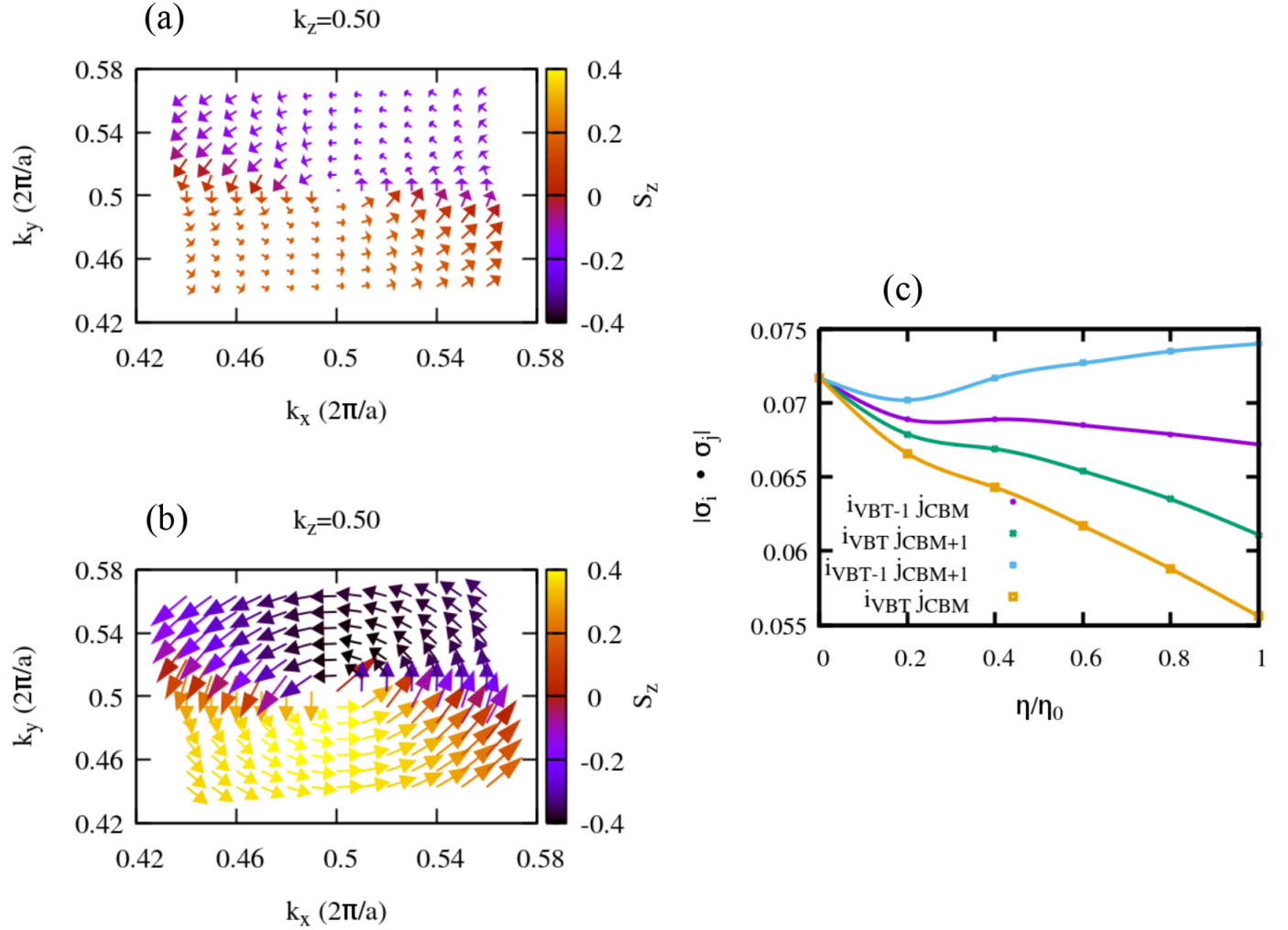


Figure 2: Spin textures for the last occupied valence band (a) and the first empty conduction one (b) in a cube with side $0.06\frac{\pi}{a}$ surrounding the R point of the BZ. A section with $z=0.5$ is shown. The third panel (c) shows the integral of four scalar products between the spin vector expectation values of a valence and a conduction state as a function of the polar distortion leading from the centrosymmetric $Pm\bar{3}m$ "S" structure ($\eta/\eta_0 = 0$) to the distorted minimum energy "A+" structure ($\eta/\eta_0 = 1$), where the inversion symmetry is broken. The last two occupied states (VBT-1 and VBT) and the first two empty ones (CBM and CBM+1) are considered.

valence band and bottom of the conduction band of the splitted bands have opposite spin orientations, reducing thus the recombination probability at the band gap. It has been recently shown, through full ab initio calculation of the spin texture,²⁷ that this picture is not

realistic for MAPbI₃, because the spin mismatch between the highest valence band and the lowest conduction bands is small and, as such, not expected to reduce the recombination rate in a significant way. In MAPbI₃ inversion symmetry is broken by a combination of orientation of the methylammonium molecular ion and the distortion it induces in the inorganic network. It is then difficult to disentangle the two effects. CsPbI₃ is a useful playground to single out the effect of the polar distortion. Calculating the spin texture in a region of the BZ close to the R point of the cubic structure we found that, as for MAPbI₃, the spin orientations are similar around the R point for the last occupied and the first empty states. We show two maps in panels (a) and (b) of Figure 2. In order to quantitatively assess the collinearity of the spins of valence and conduction states close to the band gap we show, in panel (c) of Figure 2, the integral of the modulus of the scalar product of valence/conduction spin vectors in a cube of size $0.06\frac{\text{\AA}}{a}$ around the R-point; the four possible combinations between the last two valence bands and the first two conduction ones are presented. The curves show that all the four products have similar order of magnitudes, that the lowest value is the one between the last occupied band and the first empty one and, finally, that the polar distortion does indeed enhance the spin mismatch of three out of four valence/conduction pairs.

Dynamical structural fluctuations

Next, we analyze in detail CPMD trajectories of cubic CsPbI₃ in the light of our findings on the double well potential energy surface. The trajectories were computed by Carignano *et al.* in the framework of a study⁴⁷ of the anharmonic motion of the iodine atoms in CsPbI₃ and MAPbI₃, where they showed that, at variance with FAPbI₃, these two perovskite structures are expected to have a deviation from the perfect cubic unit cell at any time of the MD, with a probability very close to 1. This hints towards the interpretation that the $Pm\bar{3}m$ symmetry can be seen as a time average, including for CsPbI₃. This phenomenon had already been reported for MAPbI₃ in earlier studies,¹⁸ where it was evidenced that the system strongly deviates from the perfectly cubic structure in the sub-picosecond time scale.

The molecular dynamics simulation were performed at 370 K under NPT-F conditions, which allow volume fluctuations by changing the supercell edges and angles. The temperature was controlled by a Nose-Hoover thermostat with three chains, and the pressure was controlled by the Martyna's barostat.⁵⁰ The time constant for both, the thermostat and barostat, was set at 50 fs. The system used for CsPbI₃ has 320 atoms (4×4×4 supercells).

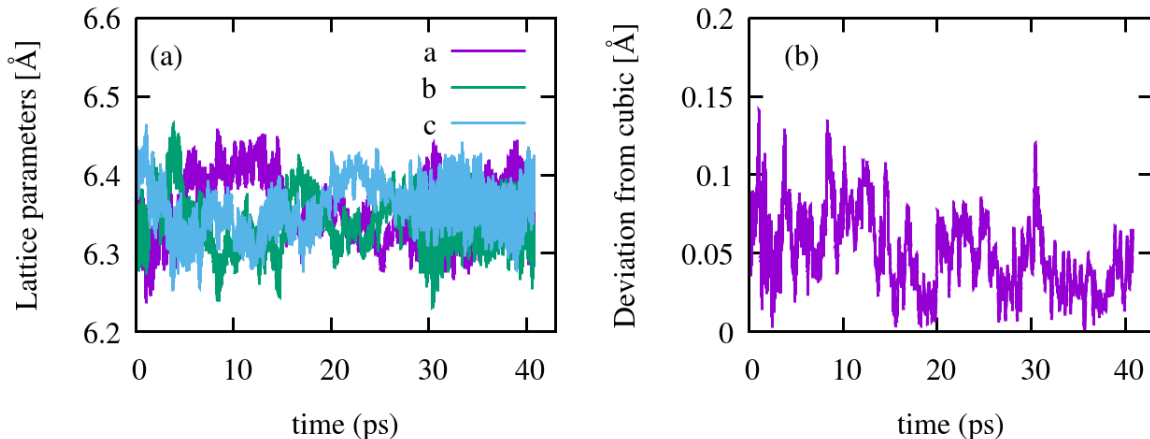


Figure 3: (a) Lattice parameters fluctuations along the CPMD trajectory at 370 K. (b) Fluctuations of the deviation from the average pseudocubic structure, as defined in Eq. 2.

In Figures 3a we show the lattice parameters fluctuations versus time. In particular, from this first simple analysis we can infer that the structure fluctuates around a cubic structure: the difference between the lattice parameters stays below 3%. Even though the structure is not perfectly cubic on average (see Table 1), the deviation from the average pseudocubic lattice structure (Figure 3b) is smaller than 1%. This deviation d is a cartesian distance obtained as:

$$d(t) = \left(\sum_{i=1}^3 (x_i(t) - \bar{x}_i)^2 \right)^{\frac{1}{2}} \quad (2)$$

where x_i are the 3 lattice parameters and \bar{x}_i their time average over the whole trajectory.

In order to analyze the MD trajectories in the light of the aforementioned double well instability, we project these trajectories onto two kind of structures: the perfectly cubic symmetric structure ("S") and the symmetry breaking structures A^+ and A^- . The chosen

Table 1: Average lattice parameters (in Angstroms) along the CPMD trajectories at 370 K and 450 K.

In Angstroms	370 K	450 K
a	6.358	6.372
b	6.338	6.391
c	6.358	6.361

approach is to study the radial distribution function of the cesium-lead pairs during the MD simulation and to compare it to our two reference structures.

Figure 4 focuses on averages over 0.5 ps intervals. At this time scale, our double well references seem to explain very well how the system explores the energy landscape. Whereas some intervals show a distance peak corresponding to the distance in the average pseudocubic structure S, for instance the [11-11.5 ps] interval shows two peaks centered on both minimum structures A^+ and A^- . This means that within 0.5 ps the structure has enough time to explore the whole double well. We think that this is the most appropriate time-scale to evidence the double well instabilities.

Dynamical Rashba effect

We now focus on the dynamical Rashba effect possibly ensuing from the nuclear dynamics exposed above. We expect to find in CsPbI_3 an effect similar to what was evidenced for MAPbI_3 for which the spatially local Rashba splitting was found to fluctuate on the subpicosecond time scale typical of the methylammonium cation dynamics.³¹

To investigate this effect, we calculate the electronic band structure, including spin-orbit coupling, at different snapshots along the trajectory. Given the results of the Pb-Cs distance analysis, we chose to focus these calculations on the [10-15 ps] interval in which we chose 50 regularly distributed snapshots (hence separated by 100 fs from each other) in order to better capture the sub pico-second dynamics. For each snapshot, we used the MD structure of the $4 \times 4 \times 4$ supercells (we remind the reader that the cell's atomic positions,

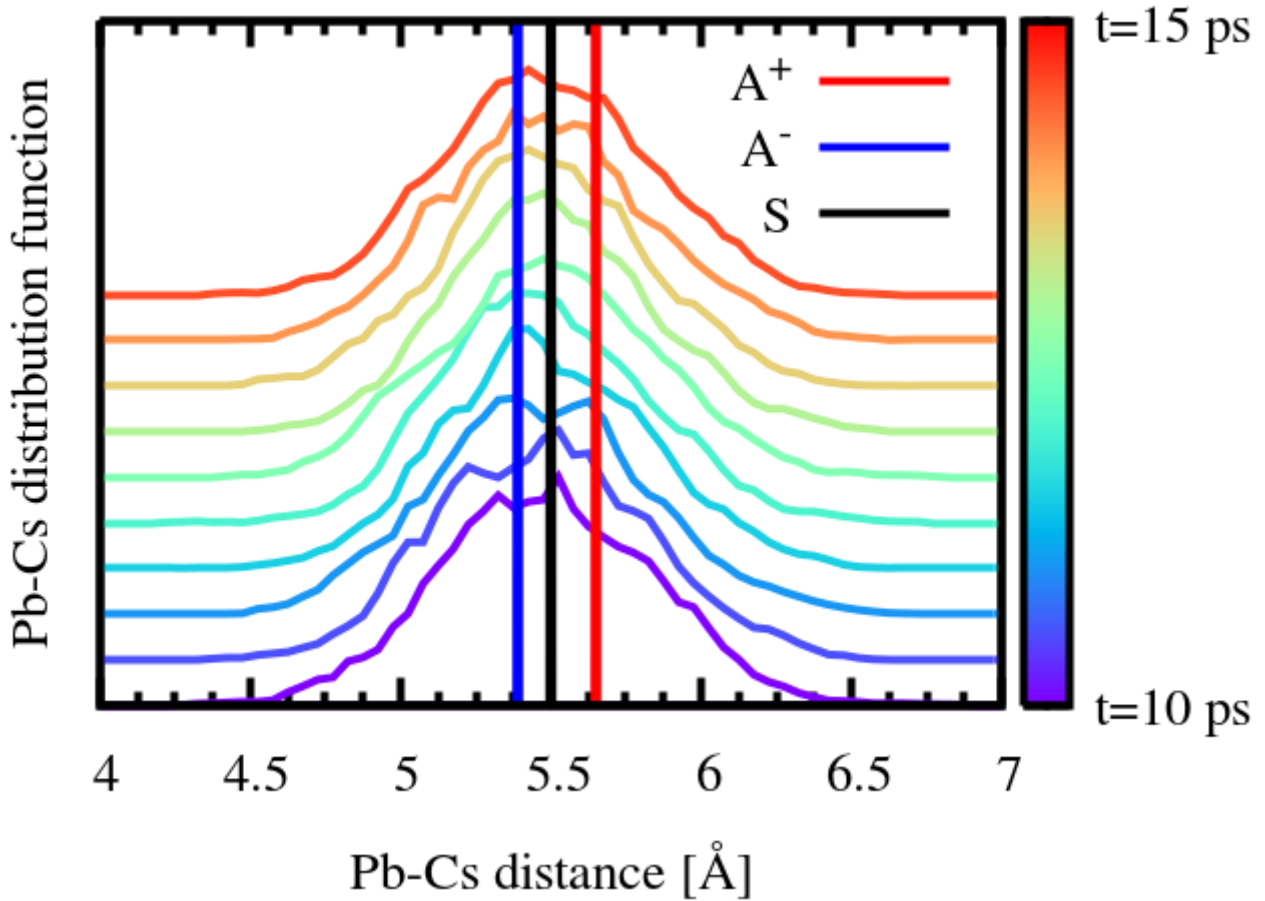


Figure 4: Distribution function of the cesium-lead pairs' distances along the MD trajectory. Here the references (vertical lines) correspond to the distances for structures S, A^+ and A^- , weighted by the ratio between the lattice parameters.

lattice parameters and angles vary) and derived its electronic band structure (see the Methods section). These calculations for $4 \times 4 \times 4$ supercells follow the guidelines of those previously done for MAPbI_3 .¹⁸

The electronic band structure calculations are done at 7 \mathbf{k} points of the Brillouin zone and, from these, parabolic bands in the vicinity of the Γ point were obtained. (For further details see the Supporting Information). In Figure 5 we plot, for each snapshot i of the 50 structures chosen in the MD trajectory and for each \mathbf{k} point, the normalized energy difference defined as:

$$\Delta E_{gap}^i(k) = [CBM^i(k) - VBT^i(k)] - [(CBM^i(\Gamma) - VBT^i(\Gamma))] \quad (3)$$

where CBM is the conduction band minimum and VBT the valence band top. This is necessary as the cell is variable along the trajectory: the fluctuations on the gap value, which are large with respect to the Rashba splitting, would mask it otherwise. The corresponding plots for the valence and conduction bands as well as the evolution of the bandgap over time are presented in the supporting information.

These results show that 100 fs is a good estimate of the timescale of the Rashba effect dynamics. Moreover, on average we see a band gap shift to the Y direction, the band gap being reduced by 1.3 meV on average. Taking the extreme case, we can infer that the amplitude of the oscillations in the 5 ps timescale is around 10 meV. Further analysis of the time coherence of the Rashba effect are provided in the supporting information file through time correlation functions.

Figure S1 shows that this is mostly due to a Rashba splitting happening at the CBM rather than at the VBT. This is coherent with the fact that the most relativistic atom, Pb, is mostly contributing to the conduction band and with what was previously reported for MAPbI₃¹⁸ as well.

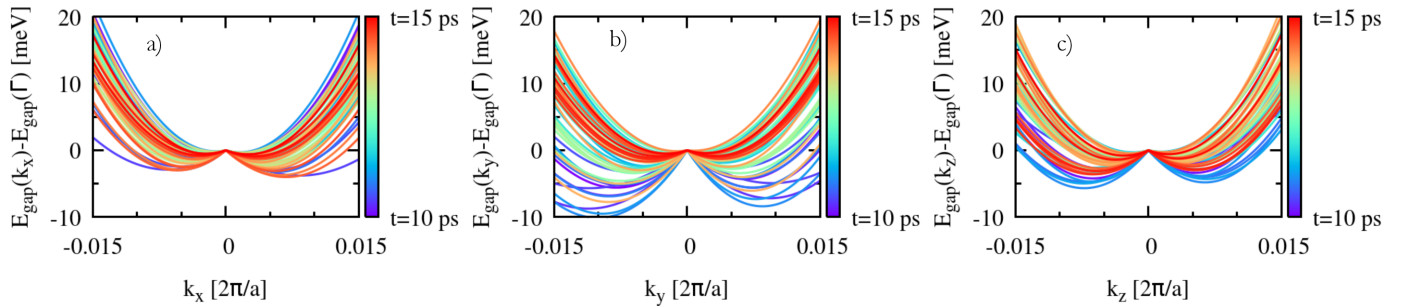


Figure 5: Differences between the gap at finite \mathbf{k} and at Γ for the 50 snapshots chosen along the MD trajectory. The three panels a-c refer to the three directions, \mathbf{k}_x , \mathbf{k}_y , \mathbf{k}_z . This difference is 0 at Γ by construction (see Eq. 3).

Figure 6a represent the oscillations of the Rashba effect in this interval through the

previously defined α parameter. This result confirms that the Rashba effect is much more substantial for the conduction band than for the valence band, and oscillates with values close to $1 \text{ eV}\cdot\text{\AA}$. Even though this is smaller than in the static case (values around $3 \text{ eV}\cdot\text{\AA}$), this means that the effect is still sizable despite the disorder induced by temperature and the large investigated supercell.

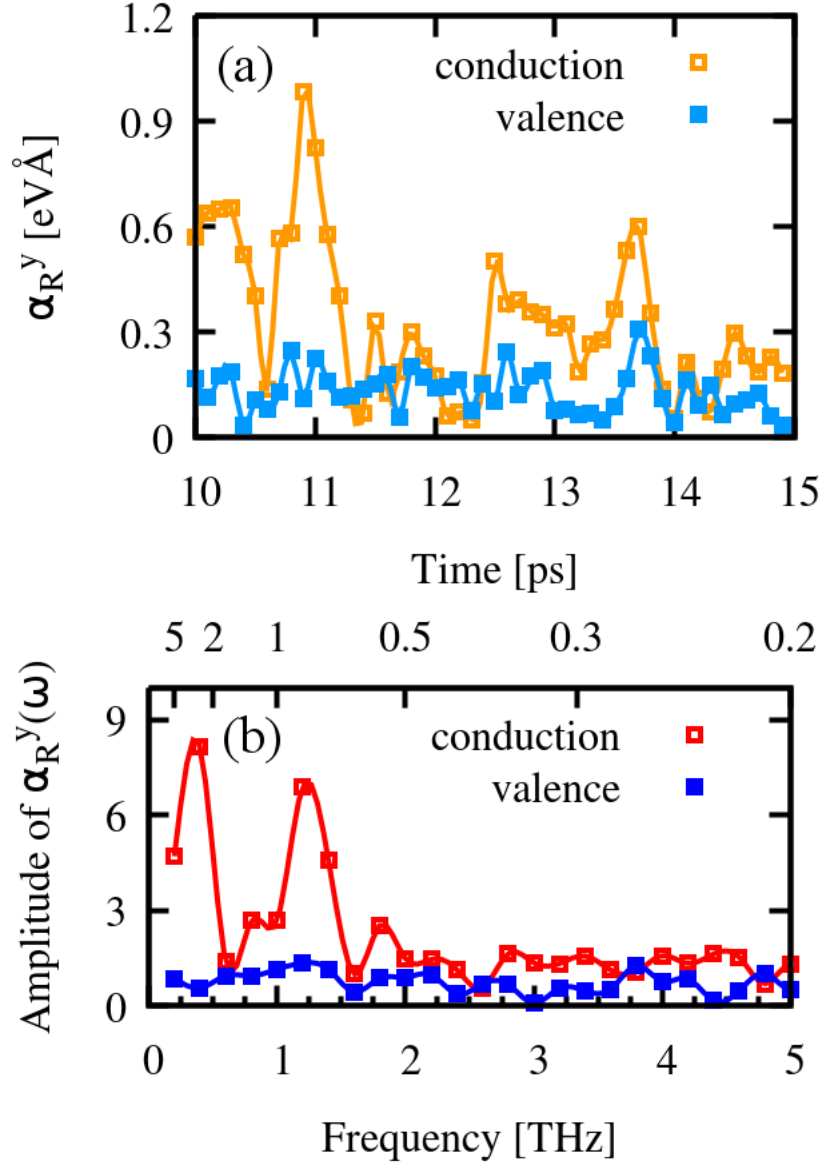


Figure 6: (a) α_R parameter for the conduction and valence bands (in the \mathbf{k}_y direction) versus time. (b) Fourier transform of the Rashba α parameter shown in panel (a).

It is interesting to further look into these oscillations through a Fourier analysis (Figure 6b) which reveals the existence of two main frequency components :

- A 2.5 ps component (frequency: 0.4 THz or 13 cm^{-1}) which could correspond to the jump through double well and thus to the slow motion of the Cs cation;
- A 0.8 ps component (frequency: 1.2 THz or 40 cm^{-1}) corresponding to the phonon modes usually associated to the Pb-I stretching (around 20-40 cm^{-1}).

We further compare the order of magnitudes of these oscillations to those obtained in a similar study lead on hybrid perovskite MAPbI₃ by Etienne *et al.*³¹ We report in Table 2 the corresponding values for the apolar structure of Ref. 31, because a Cs atom has no permanent dipole moment. Note that nevertheless, for the polar structure, the largest α value reported in Ref. 31 (10.36) is even smaller than the largest one reported for the non-polar structure. One needs to keep in mind that we have here very large supercells compared to what was used in that study. The conclusion we can draw from this comparison is that we observe a sizable dynamical Rashba effect even with large supercells and the absence of the organic molecule, which in general is a possible source of symmetry breaking in these halide perovskite structures. The fact that the order of magnitude of the dynamical Rashba splitting is similar for MAPbI₃ and CsPbI₃ is in agreement with the recent observation of similar recombination kinetics for both compounds.⁵¹

Table 2: Maximum value of the α oscillations.

Number of formula units	α for hybrid MAPbI ₃ from Ref. 31 (eV.Å)	α for inorganic CsPbI ₃ from our results (eV.Å)
1	12.48	
4	3.86	
32	2.19	
64		0.96

Concluding remarks

In summary, we investigated the effect of spatial and temporal disorder on the Rashba splitting in the cubic α phase of inorganic halide perovskite CsPbI₃. The analysis focused on the fluctuations of the Rashba α -parameter—a measure of the Rashba band splitting—along a molecular dynamics trajectory for a large supercell.⁴⁷ Our results highlight a dynamical Rashba effect similar to the one previously observed for hybrid organic-inorganic halide perovskites,³¹ which persists in spite of the quenching effect coming from spatial disorder in this relatively large simulation cell (320 atoms). Some low-frequency vibrational modes of the system, and in particular the anharmonic behavior, which has been shown to originate from the double well potential energy landscape of a polar optical phonon,⁴⁵ contribute to the spatial extension of the Rashba effect. This is confirmed by the Fourier analysis of the Rashba α -parameter fluctuations.

An expected consequence of the Rashba effect is the reduction of the carriers recombination rate⁹ and consequent enhancement of their radiative lifetime; however, this effect is submitted to a specific spin texture which has been recently shown not to occur in MAPbI₃. Our calculated ab initio spin textures in CsPbI₃ suggest that, although a reduction of the recombination rate due to Rashba splitting is indeed expected, its effect is not as large as previous model calculations had predicted.

Methods

Density functional theory for band structure calculations

In this study we started from the minimum reference structures obtained in Ref. 45 which were optimized with the PBE functional letting both the lattice parameters and the atomic positions relax, keeping the cell's angles fixed. These structures are thus slightly orthorhombic (0.6% distortion). The total energy gain due to the polar distortion is smaller with

PBE (3.4 meV) than with LDA, as reported in Ref. 46 with and without SOC and slightly different settings, but with an analogous energy profile.

For these reference structures, geometry optimizations and force calculations were performed with spin-orbit coupling (SOC). Fully relativistic pseudopotentials were used, with the Cs [$5s^25p^66s^1$], I [$5s^25p^5$] and Pb [$5d^{10}6s^26p^2$] electrons treated as valence states. The choice of 14 electrons for Pb and 9 for Cs was previously discussed.⁴⁵ PBE pseudopotentials are ultrasoft ones and were used with a wave function energy cutoff of 25 Ry (200 Ry for the charge density). LDA ones were norm conserving and were used with a 70 Ry wave function cutoff energy.

In order to investigate the effect of spatial and dynamical disorder on the Rashba effect, we proceeded with the following two steps:

- as for the study of the spatial domains, the band structure calculations of the constructed $2\times 1\times 1$ and $1\times 1\times 2$ supercells were performed with fully relativistic pseudopotentials (for Pb and I) with PBE and SOC. The same calculations were made also with LDA and showed qualitatively similar results.
- in order to study the dynamical Rashba effect from CPMD, the band structure calculations were performed with the same fully relativistic US pseudopotentials using the PBE xc functional, in coherence with the CPMD calculations from which MD trajectories were taken,⁴⁷ which were done using PBE as well (with the CP2K code).

Spin textures were calculated by obtaining the expectation value of the spin operators in the three cartesian directions on a single particle Kohn-Sham wave function ($S_i^\alpha = \langle \psi_i | \sigma_\alpha | \psi_i \rangle$, where $\sigma_\alpha, \alpha = 1, 2, 3$ are the three Pauli spin matrices, ψ_i is a two component spinor eigenfunction). The Brillouin zone was sampled with Γ -centered Monkhorst-Pack meshes⁵² with subdivisions of $8\times 8\times 8$ k-points for unit cells, and corresponding sampling when doubling the cell in x or z directions. The molecular dynamics snapshots were sampled with the Γ point only.

Associated Content

The authors declare no competing financial interest.

Acknowledgement

Dr. Arthur Marronnier's PhD project was funded by the Graduate School of École des Ponts ParisTech and the French Department of Energy (MTES). HPC resources of TGCC and CINES were used through allocation 2017090642 and x20170906724 GENCI projects. The work at FOTON and ISCR was funded by the European Union's Horizon 2020 program, through a FET Open research and innovation action under the grant agreement No 687008.

Supporting Information Available

The following files are available free of charge.

We provide in the supporting information additional results on the effect of dynamical disorder on the conduction band minimum and valence band top throughout the chosen 5 ps interval of study for our band structure calculations. We also provide an analysis of the time correlation of the Rashba parameter α (or α_R) and of the spin textures.

References

- (1) Sanehira, E. M.; Marshall, A. R.; Christians, J. A.; Harvey, S. P.; Ciesielski, P. N.; Wheeler, L. M.; Schulz, P.; Lin, L. Y.; Beard, M. C.; Luther, J. M. Enhanced mobility CsPbI₃ quantum dot arrays for record-efficiency, high-voltage photovoltaic cells. *Science Advances* **2017**, *3*.
- (2) Wang, K.; Jin, Z.; Liang, L.; Bian, H.; Bai, D.; Wang, H.; Zhang, J.; Wang, Q.;

- Shengzhong, L. All-inorganic cesium lead iodide perovskite solar cells with stabilized efficiency beyond 15% . *Nature Communications* **2018**, *9*, 4544.
- (3) Saliba, M.; Matsui, T.; Seo, J.-Y.; Domanski, K.; Correa-Baena, J.-P.; Nazeeruddin, M. K.; Zakeeruddin, S. M.; Tress, W.; Abate, A.; Hagfeldt, A.; Grätzel, M. Cesium-containing Triple Cation Perovskite Solar Cells: Improved Stability, Reproducibility and High Efficiency. *Energy Environ. Sci.* **2016**, *9*, 1989–1997.
- (4) Chiarella, F.; Zappettini, A.; Licci, F.; Borriello, I.; Cantele, G.; Ninno, D.; Cassinese, A.; Vaglio, R. Combined experimental and theoretical investigation of optical, structural, and electronic properties of $\text{CH}_3\text{NH}_3\text{SnX}_3$ thin films (X= Cl, Br). *Physical Review B* **2008**, *77*, 045129.
- (5) Ogomi, Y.; Morita, A.; Tsukamoto, S.; Saitho, T.; Fujikawa, N.; Shen, Q.; Toyoda, T.; Yoshino, K.; Pandey, S. S.; Ma, T., et al. $\text{CH}_3\text{NH}_3\text{Sn}_x\text{Pb}_{(1-x)}\text{I}_3$ Perovskite solar cells covering up to 1060 nm. *The journal of physical chemistry letters* **2014**, *5*, 1004–1011.
- (6) Eperon, G. E.; Stranks, S. D.; Menelaou, C.; Johnston, M. B.; Herz, L. M.; Snaith, H. J. Formamidinium Lead Trihalide: a Broadly Tunable Perovskite for Efficient Planar Heterojunction Solar Cells. *Energy Environ. Sci.* **2014**, *7*, 982.
- (7) Stoumpos, C. C.; Malliakas, C. D.; Kanatzidis, M. G. Semiconducting Tin and Lead Iodide Perovskites with Organic Cations: Phase Transitions, High Mobilities, and Near-Infrared Photoluminescent Properties. *Inorg. Chem.* **2013**, *52*, 9019–9038.
- (8) Wehrenfennig, C.; Liu, M.; Snaith, H. J.; Johnston, M. B.; Herz, L. M. Charge-carrier dynamics in vapour-deposited films of the organolead halide perovskite $\text{CH}_3\text{NH}_3\text{PbI}_{3-x}\text{Cl}_x$. *Energy & Environmental Science* **2014**, *7*, 2269–2275.
- (9) Zheng, F.; Tan, L. Z.; Liu, S.; Rappe, A. M. Rashba spin-orbit coupling enhanced carrier lifetime in $\text{CH}_3\text{NH}_3\text{PbI}_3$. *Nano Lett.* **2015**, *15*, 7794–7800.

- (10) Ponseca Jr, C. S.; Savenije, T. J.; Abdellah, M.; Zheng, K.; Yartsev, A.; Pascher, T.; Harlang, T.; Chabera, P.; Pullerits, T.; Stepanov, A., et al. Organometal halide perovskite solar cell materials rationalized: ultrafast charge generation, high and microsecond-long balanced mobilities, and slow recombination. *J. Am. Chem. Soc.* **2014**, *136*, 5189–5192.
- (11) Cahen, D.; Edri, E.; Hodes, G.; Gartsman, K.; Kirmayer, S.; Mukhopadhyay, S. Elucidating the charge carrier separation and working mechanism of CH₃NH₃PbI_{3-x}Cl_x perovskite solar cells. *Nature communications* **2014**, *5*, 3461.
- (12) Xing, G.; Mathews, N.; Sun, S.; Lim, S. S.; Lam, Y. M.; Grätzel, M.; Mhaisalkar, S.; Sum, T. C. Long-range balanced electron-and hole-transport lengths in organic-inorganic CH₃NH₃PbI₃. *Science* **2013**, *342*, 344–347.
- (13) Stranks, S. D.; Eperon, G. E.; Grancini, G.; Menelaou, C.; Alcocer, M. J.; Leijtens, T.; Herz, L. M.; Petrozza, A.; Snaith, H. J. Electron-hole diffusion lengths exceeding 1 micrometer in an organometal trihalide perovskite absorber. *Science* **2013**, *342*, 341–344.
- (14) Lee, H.; Gaiaschi, S.; Chapon, P.; Marronnier, A.; Lee, H.; Vanel, J.-C.; Tondelier, D.; Boureé, J.-E.; Bonmassieux, Y.; Geffroy, B. Direct Experimental Evidence of Halide Ionic Migration under Bias in CH₃NH₃PbI_{3-x}Cl_x-Based Perovskite Solar Cells Using GD-OES Analysis. *ACS Energy Letters* **2017**, *2*, 943–949.
- (15) Yang, T.-Y.; Gregori, G.; Pellet, N.; Grätzel, M.; Maier, J. The significance of ion conduction in a hybrid organic–inorganic lead-iodide-based perovskite photosensitizer. *Angewandte Chemie* **2015**, *127*, 8016–8021.
- (16) Even, J.; Pedesseau, L.; Katan, C. Analysis of multivalley and multibandgap absorption and enhancement of free carriers related to exciton screening in hybrid perovskites. *The Journal of Physical Chemistry C* **2014**, *118*, 11566–11572.

- (17) Ma, J.; Wang, L.-W. Nanoscale charge localization induced by random orientations of organic molecules in hybrid perovskite CH₃NH₃PbI₃. *Nano Lett.* **2014**, *15*, 248–253.
- (18) Quarti, C.; Mosconi, E.; Ball, J. M.; D’Innocenzo, V.; Tao, C.; Pathak, S.; Snaith, H. J.; Petrozza, A.; De Angelis, F. Structural and optical properties of methylammonium lead iodide across the tetragonal to cubic phase transition: implications for perovskite solar cells. *Energy Environ. Sci.* **2016**, *9*, 155–163.
- (19) Davies, C. L.; Filip, M. R.; Patel, J. B.; Crothers, T. W.; Verdi, C.; Wright, A. D.; Milot, R. L.; Giustino, F.; Johnston, M. B.; Herz, L. M. Bimolecular recombination in methylammonium lead triiodide perovskite is an inverse absorption process. *Nature Communications* **2018**, *9*, 293–.
- (20) Even, J.; Pedesseau, L.; Jancu, J.-M.; Katan, C. Importance of spin–orbit coupling in hybrid organic/inorganic perovskites for photovoltaic applications. *The Journal of Physical Chemistry Letters* **2013**, *4*, 2999–3005.
- (21) Kim, M.; Im, J.; Freeman, A. J.; Ihm, J.; Jin, H. Switchable $S = 1/2$ and $J = 1/2$ Rashba bands in ferroelectric halide perovskites. *Proceedings of the National Academy of Sciences* **2014**, *111*, 6900–6904.
- (22) Even, J.; Pedesseau, L.; Jancu, J.-M.; Katan, C. DFT and k·p Modelling of the Phase Transitions of Lead and Tin Halide Perovskites for Photovoltaic Cells. *Phys. Status Solidi RRL* **2014**, *8*, 31–35.
- (23) Amat, A.; Mosconi, E.; Ronca, E.; Quarti, C.; Umari, P.; Nazeeruddin, M. K.; Grätzel, M.; De Angelis, F. Cation-Induced Band-Gap Tuning in Organohalide Perovskites: Interplay of Spin–Orbit Coupling and Octahedra Tilting. *Nano Lett.* **2014**, *14*, 3608–3616.
- (24) Brivio, F.; Butler, K. T.; Walsh, A.; van Schilfgaarde, M. Relativistic quasiparticle

- self-consistent electronic structure of hybrid halide perovskite photovoltaic absorbers. *Phys. Rev. B* **2014**, *89*, 155204.
- (25) Zhang, X.; Liu, Q.; Luo, J.-W.; Freeman, A. J.; Zunger, A. Hidden spin polarization in inversion-symmetric bulk crystals. *Nature Physics* **2014**, *10*, 387.
- (26) Kепенekian, M.; Robles, R.; Katan, C.; Saponi, D.; Pedesseau, L.; Even, J. Rashba and Dresselhaus Effects in Hybrid Organic–Inorganic Perovskites: From Basics to Devices. *ACS Nano* **2015**, *9*, 11557–11567, PMID: 26348023.
- (27) Zhang, X.; Shen, J.-X.; Van de Walle, C. G. Three-Dimensional Spin Texture in Hybrid Perovskites and Its Impact on Optical Transitions. *The Journal of Physical Chemistry Letters* **2018**, *9*, 2903–2908, PMID: 29763326.
- (28) Zhang, X.; Shen, J.-X.; Wang, W.; Van de Walle, C. G. First-Principles Analysis of Radiative Recombination in Lead-Halide Perovskites. *ACS Energy Letters* **2018**, *3*, 2329–2334.
- (29) Yu, Z.-G. Rashba Effect and Carrier Mobility in Hybrid Organic-Inorganic Perovskites. *The Journal of Physical Chemistry Letters* **2016**, *7*, 3078–3083, PMID: 27459897.
- (30) Kang, Y.; Han, S. Intrinsic Carrier Mobility of Cesium Lead Halide Perovskites. *Phys. Rev. Applied* **2018**, *10*, 044013.
- (31) Etienne, T.; Mosconi, E.; De Angelis, F. Dynamical Origin of the Rashba Effect in Organohalide Lead Perovskites: A Key to Suppressed Carrier Recombination in Perovskite Solar Cells? *J. Phys. Chem. Lett.* **2016**, *7*, 1638–1645.
- (32) Hutter, E. M.; Savenjie, T. J. Thermally Activated Second-Order Recombination Hints toward Indirect Recombination in Fully Inorganic CsPbI₃ Perovskites. **2018**, *3*, 2068–2069.

- (33) Frohna, K.; Deshpande, T.; Harter, J.; Peng, W.; Barker, B. A.; Neaton, J. B.; Louie, S. G.; Bakr, O. M.; Hsieh, D.; Bernardi, M. Inversion symmetry and bulk Rashba effect in methylammonium lead iodide perovskite single crystals. *Nature Communications* **2018**, *9*, 1829.
- (34) Niesner, D.; Hauck, M.; Shrestha, S.; Levchuk, I.; Matt, G. J.; Osvet, A.; Bantenschuk, M.; Brabec, C.; Weber, H. B.; Fauster, T. Structural fluctuations cause spin-split states in tetragonal (CH₃NH₃)PbI₃ as evidenced by the circular photogalvanic effect. *PNAS* **2018**, *115*, 9509–9514.
- (35) Katan, C.; Mohite, A. D.; Even, J. Riddles in perovskite research. *Nat. Mater.* **2018**, *17*, 377–384.
- (36) Fujii, Y.; Hoshino, S.; Yamada, Y.; Shirane, G. Neutron-scattering Study on Phase Transitions of CsPbCl₃. *Phys. Rev. B* **1974**, *9*, 4549–4559.
- (37) Trots, D.; Myagkota, S. High-temperature Structural Evolution of Caesium and Rubidium Triiodoplumbates. *J. Phys. Chem. Solids* **2008**, *69*, 2520–2526.
- (38) Hutton, J.; Nelmes, R.; Meyer, G.; Eiriksson, V. High-resolution studies of cubic perovskites by elastic neutron diffraction: CsPbCl₃. *Journal of Physics C: Solid State Physics* **1979**, *12*, 5393.
- (39) Even, J.; Carignano, M.; Katan, C. Molecular Disorder and Translation/Rotation Coupling in the Plastic Crystal Phase of Hybrid Perovskites. *Nanoscale* **2016**, *8*, 6222–6236.
- (40) Yaffe, O.; Guo, Y.; Tan, L. Z.; Egger, D. A.; Hull, T.; Stoumpos, C. C.; Zheng, F.; Heinz, T. F.; Kronik, L.; Kanatzidis, M. G., et al. Local polar fluctuations in lead halide perovskite crystals. *Phys. Rev. Lett.* **2017**, *118*, 136001.
- (41) Marronnier, A.; Lee, H.; Lee, H.; Kim, M.; Eypert, C.; Gaston, J.-P.; Roma, G.; Tondelier, D.; Geffroy, B.; Bonnassieux, Y. Electrical and Optical Degradation Study of

- Methylammonium-based Perovskite Materials under Ambient Conditions. *Sol. Energy Mater. Sol. Cells* **2018**, *178*, 179–185.
- (42) Anusca, I.; Balčiūnas, S.; Gemeiner, P.; Svirskas, Š.; Sanlialp, M.; Lackner, G.; Fettkenhauer, C.; Belovickis, J.; Samulionis, V.; Ivanov, M., et al. Dielectric response: Answer to many questions in the methylammonium lead halide solar cell absorbers. *Advanced Energy Materials* **2017**, *7*, 1700600.
- (43) Sendner, M.; Nayak, P. K.; Egger, D. A.; Beck, S.; Müller, C.; Epping, B.; Kowalsky, W.; Kronik, L.; Snaith, H. J.; Pucci, A.; Lovrinčić, R. Optical phonons in methylammonium lead halide perovskites and implications for charge transport. *Mater. Horiz.* **2016**, *3*, 613–620.
- (44) Fu, M.; Tamarat, P.; Trebbia, J.-B.; Bodnarchuk, M. I.; Kovalenko, M. V.; Even, J.; Lounis, B. Unraveling exciton–phonon coupling in individual FAPbI₃ nanocrystals emitting near-infrared single photons. *Nature communications* **2018**, *9*, 3318.
- (45) Marronnier, A.; Lee, H.; Geffroy, B.; Even, J.; Bonnassieux, Y.; Roma, G. Structural Instabilities Related to Highly Anharmonic Phonons in Halide Perovskites. *J. Phys. Chem. Lett.* **2017**, *8*, 2659–2665.
- (46) Marronnier, A.; Roma, G.; Boyer-Richard, S.; Pedesseau, L.; Jancu, J.-M.; Bonnassieux, Y.; Katan, C.; Stoumpos, C. C.; Kanatzidis, M. G.; Even, J. Anharmonicity and Disorder in the Black Phases of Cesium Lead Iodide Used for Stable Inorganic Perovskite Solar Cells. *ACS Nano* **2018**, *12*, 3477–3486.
- (47) Carignano, M. A.; Aravindh, S. A.; Roqan, I. S.; Even, J.; Katan, C. Critical Fluctuations and Anharmonicity in Lead Iodide Perovskites from Molecular Dynamics Supercell Simulations. *The Journal of Physical Chemistry C* **2017**, *121*, 20729–20738.
- (48) Picozzi, S. Ferroelectric Rashba semiconductors as a novel class of multifunctional materials. *Frontiers in Physics* **2014**, *2*, 10.

- (49) Krempaský, J. et al. Disentangling bulk and surface Rashba effects in ferroelectric α -GeTe. *Phys. Rev. B* **2016**, *94*, 205111.
- (50) Martyna, G. J.; Tuckerman, M. E.; Tobias, D. J.; Klein, M. L. Explicit reversible integrators for extended systems dynamics. *Mol. Phys.* **1996**, *87*, 1117–1157.
- (51) Dastidar, S.; Li, S.; Smolin, S. Y.; Baxter, J. B.; Fafarman, A. T. Slow Electron-Hole Recombination in Lead Iodide Perovskites Does Not Require a Molecular Dipole. *ACS Energy Letters* **2017**, *2*, 2239–2244.
- (52) Monkhorst, H. J.; Pack, J. D. Special points for Brillouin-zone integrations. *Physical review B* **1976**, *13*, 5188.

Graphical TOC Entry

